First measurement of the magnetic field on FK Com and its relation to the contemporaneous star-spot locations⋆

H. Korhonen,[1]† S. Hubrig,[2] S. V. Berdyugina,[3,4] Th. Granzer,[5] T. Hackman,[6] M. Schöller,[1] K. G. Strassmeier[5] and M. Weber[5]

[1]*European Southern Observatory, Karl-Schwarzschild-Str 2, D-85748 Garching bei München, Germany*
[2]*European Southern Observatory, Casilla 19001, Santiago, Chile*
[3]*Kiepenheuer Institut für Sonnenphysik, D-79104 Freiburg, Germany*
[4]*Institute of Astronomy, ETH Zürich, 8093 Zürich, Switzerland*
[5]*Astrophysikalisches Institut Potsdam, An der Sternwarte 16, D-14882 Potsdam, Germany*
[6]*Observatory, PO Box 14, FI-00014 University of Helsinki, Finland*

ABSTRACT

In this study, we present simultaneous low-resolution longitudinal magnetic field measurements and high-resolution spectroscopic observations of the cool single giant FK Com. The variation of the magnetic field over the rotational period of 2.4 d is compared with the star-spot location obtained using Doppler imaging techniques, V-band photometry and $V - I$ colours. The chromospheric activity is studied simultaneously with the photospheric activity using high-resolution observations of the Hα, Hβ and Hγ line profiles. Both the maximum (272 ± 24 G) and minimum (60 ± 17 G) in the mean longitudinal magnetic field, $\langle B_z \rangle$, are detected close to the phases where cool spots appear on the stellar surface. A possible explanation for such a behaviour is that the active regions at the two longitudes separated by 0.2 in phase have opposite polarities.

Key words: stars: activity – stars: individual: FK Comae Berenices – stars: late-type – stars: magnetic fields – stars: spots.

1 INTRODUCTION

The strongest magnetic fields in non-degenerate stars are measured in Ap stars (see e.g. Babcock 1960; Landstreet 1992; Hubrig et al. 2005). The development of spectropolarimetric techniques in the last years has enabled us to detect the weaker stellar magnetic fields seen in many cool stars, and to study the topologies of their magnetic fields in detail using the Zeeman–Doppler imaging.

The Zeeman–Doppler imaging (Semel 1989) is closely related to traditional Doppler imaging (see e.g. Vogt, Penrod & Hatzes 1987; Piskunov, Tuominen & Vilhu 1990), where high-resolution, high signal-to-noise ratio (S/N) spectra at different rotational phases of a star are used to measure the rotationally modulated distortions in the line profiles. These distortions are produced by the inhomogeneous distribution of the observed characteristic, e.g. effective temperature or elemental abundance. Surface maps, the so-called Doppler images, are constructed by combining all the observations from different rotational phases and comparing them with synthetic model line profiles. In the Zeeman–Doppler imaging, similar techniques are used, but the observations consist of high-resolution spectropolarimetric observations, including either circular polarization (Stokes V) or preferably the full Stokes vector. Using this technique, different types of stars have been mapped: young rapid rotators (e.g. Donati et al. 2003; Marsden et al. 2006), more evolved stars (e.g. Donati et al. 2003; Petit et al. 2004) and M dwarfs (e.g. Donati et al. 2006).

The Zeeman–Doppler imaging provides detailed maps of the stellar surface magnetic fields, but observationally this technique is very demanding as high-resolution, high S/N observations in polarized light are needed. On the other hand, information on the longitudinal magnetic field also can be obtained using low-resolution spectropolarimetric observations in circular polarization (see e.g. Hubrig et al. 2006a). With such observations, we can retrieve the component of the magnetic field parallel to the line-of-sight, weighted by the local emergent spectral line intensity and averaged over the stellar hemisphere visible at the time of observation. Due to the low resolution, such spectropolarimetric observations, however, do not provide a detailed insight into the magnetic surface structure since the polarized line profiles of temperature and magnetic-field-sensitive lines cannot be studied individually.

Here, we present the first study of the mean longitudinal magnetic field of FK Com, which is the prototype of the small class of FK

Comae stars (Bopp & Stencel 1981). These stars are magnetically very active late-type giants with photometric and spectroscopic characteristics similar to those of the very active RS CVn stars. The main difference between the groups is that the RS CVn stars are close binary systems in which the tidal effects produce synchronous rotation, and therefore also rapid rotation, whereas the FK Comae stars do not show significant radial velocity variations caused by a companion, and are thus most likely single stars.

FK Com itself, with its $v \sin i$ of $160 \, \mathrm{km \, s^{-1}}$, is the fastest rotator of the FK Comae stars, and hence also the most active in this group. The spectrum of FK Com was first described by Merrill (1948). He noted a large projected rotational velocity, Hα and Ca II H&K emission, and the variability of the Hα profile. Due to the very broad line profiles, the radial velocity of FK Com is difficult to measure very accurately, leaving still some room to speculate on its possible binarity. The radial velocity variations have been constrained to $\pm 3 \, \mathrm{km \, s^{-1}}$ by Huenemoerder et al. (1993), giving very strict limits to the mass of the possible companion. Small visual brightness variations in FK Com of ~ 0.1 mag in the V band with a period of 2.412 d were first reported by Chugainov (1966). These variations are interpreted to be caused by large star-spots on the surface. Several surface temperature maps of FK Com have been obtained over the years using the Doppler imaging technique (see e.g. Korhonen et al. 1999, 2007). These surface temperature maps mainly show high-latitude spots with spot temperatures of typically 1000 K less than that of the unspotted surface.

The current work provides the first measurement of the magnetic field on FK Com. The low-resolution spectropolarimetric observations in circular polarization are used to infer the behaviour of the mean longitudinal magnetic field at different rotational phases. The Doppler imaging technique is applied to the high-resolution spectra to construct a simultaneous surface temperature map. The longitudinal magnetic field measurements are compared to the contemporaneous star-spot locations obtained from the surface image and the chromospheric activity seen in the Hα, Hβ and Hγ lines.

2 OBSERVATIONS AND DATA ANALYSIS

Low-resolution spectropolarimetric observations were obtained at the European Southern Observatory with FORS 1 (FOcal Reducer low dispersion Spectrograph; see Appenzeller et al. 1998) mounted on the 8-m Kueyen telescope of the VLT. For the Doppler imaging, the high-resolution spectra in integral light were observed at the fully robotic 1.2-m STELLA observatory in Tenerife (see e.g. Strassmeier et al. 2004; Weber et al. 2008). Photometric observations in the V and I bands were obtained with the Vienna automatic photometric telescope Amadeus in Arizona (e.g. Strassmeier et al. 1997; Granzer, Reegen & Strassmeier 2001). The phases for all the observations were calculated using the ephemeris obtained from 25 years of photometric observations, $\mathrm{HJD} = 243\,9252.895 + (2.400\,2466 \pm 0.000\,0056 \, \mathrm{d})E$, referring to a photometric minimum and period calculated by Jetsu, Pelt & Tuominen (1993).

All the observations from different sites used in this work are overlapping in time, but they have rather different time-spans. The high-resolution spectroscopy from the STELLA observatory is taken over just two stellar rotations, whereas the spectropolarimetry with FORS 1 is from almost six rotations and the photometric observations extend over 16 stellar rotations. The basis for using observations from so vastly varying time periods is that the spot configuration does not change significantly during this time. The stability of the surface structures is discussed in detail in Section 4.1.

2.1 Spectropolarimetry

FORS 1 is a multimode instrument equipped with polarization analysing optics comprising super-achromatic half-wave and quarter-wave phase retarder plates, and a Wollaston prism with a beam divergence of 22 arcsec in standard-resolution mode. Spectropolarimetric observations were obtained between 2008 April 12 and April 26, using GRISM 600B and a 0.4 arcsec slit, resulting in a resolving power ($\lambda / \Delta\lambda$) of ~ 2000 and a wavelength coverage of 3250–6215 Å. We used a non-standard readout mode (200 kHz, low, 1×1), which provided a broader dynamic range, hence allowing us to increase the S/N of individual spectra. To minimize the cross-talk effect, we executed the sequence of sub-exposures $+45 - 45$, $+45 - 45$, $+45 - 45$, etc. up to six times and calculated the values V/I using

$$\frac{V}{I} = \frac{1}{2} \left\{ \left(\frac{f^{\mathrm{o}} - f^{\mathrm{e}}}{f^{\mathrm{o}} + f^{\mathrm{e}}} \right)_{\alpha = -45^\circ} - \left(\frac{f^{\mathrm{o}} - f^{\mathrm{e}}}{f^{\mathrm{o}} + f^{\mathrm{e}}} \right)_{\alpha = +45^\circ} \right\}, \tag{1}$$

where α gives the position angle of the retarder waveplate and f^{o} and f^{e} are ordinary and extraordinary beams, respectively. Stokes I values have been obtained from the sum of the ordinary and extraordinary beams. The typical exposure time for each sub-exposure was about 120 s. The achieved S/N for the whole sequences of sub-exposures were in the range from 2200 to 2500. More details on the observing technique with FORS 1 can be found, e.g. in Hubrig et al. (2004).

The mean longitudinal magnetic field is diagnosed from the slope of a linear regression of V/I versus the quantity

$$-\frac{g_{\mathrm{eff}} e}{4\pi m_e c^2} \lambda^2 \frac{1}{I} \frac{\mathrm{d}I}{\mathrm{d}\lambda} \langle B_z \rangle + V_0 / I_0, \tag{2}$$

where V is the Stokes parameter which measures the circular polarization, I is the intensity observed in unpolarized light, g_{eff} is the effective Landé factor, e is the electron charge, m_e is the electron mass, c is the speed of light, λ is the wavelength, $\mathrm{d}I/\mathrm{d}\lambda$ is the derivative of Stokes I and $\langle B_z \rangle$ is the mean longitudinal field. Our experience from a study of a large sample of magnetic and non-magnetic Ap and Bp stars revealed that this regression technique is very robust and that detections with $B_z > 3\sigma$ result only for stars possessing magnetic fields (see e.g. Hubrig et al. 2006b).

In Fig. 1, we show an example of Stokes I and V spectra of FK Com in the spectral region around the line Fe I λ 4668 Å at the time of the field maximum of the longitudinal magnetic field. The values for the longitudinal magnetic field are measured using all the lines in the spectra. When $\langle B_z \rangle$ is plotted over the rotational phase, a clear variation of the field is seen, with the maximum value $\langle B_z \rangle = 272 \pm 24$ G at the phase 0.08 and the field minimum $\langle B_z \rangle = 60 \pm 17$ G at the phase 0.36 (see Fig. 2). In Table 1, we list the dates of observations, corresponding rotational phases and our measurements with 1σ uncertainties.

2.2 High-resolution spectroscopy

The high-resolution spectroscopic observations used for the Doppler imaging and investigating Hα variations were obtained with the STELLA-I robotic telescope between 2008 April 14 and April 19. The fibre-fed STELLA Echelle Spectrograph (SES) spectrograph provides a resolving power ($\lambda / \Delta\lambda$) of 55 000 and a wavelength coverage of 3900–9000 Å in a fixed spectral format. The exposure time was always 3600 s, and it provided an average S/N of 115 per resolution element in the Doppler imaging region around 6400 Å. The spectra were reduced using the SES reduction pipeline
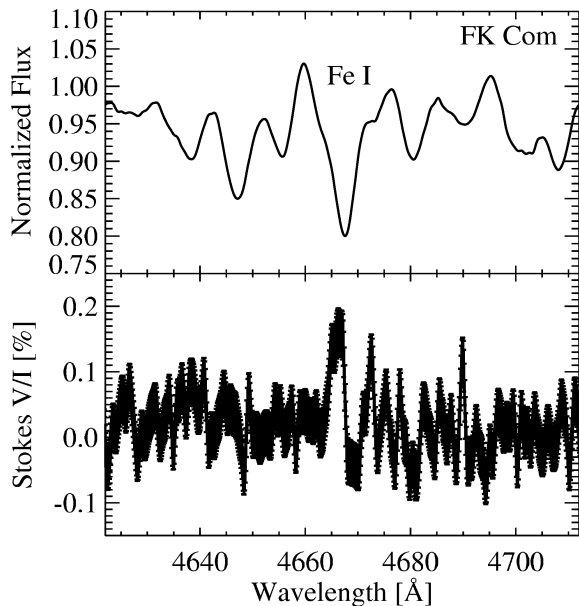
Figure 1. An example of FORS 1 Stokes *I* and *V* spectra of FK Com in the spectral region around the line Fe I λ 4668 Å at the time of the maximum of the longitudinal magnetic field. The thickness of the plotted lines in the Stokes *V* spectra corresponds to the uncertainty of the measurement of polarization determined from photon noise.
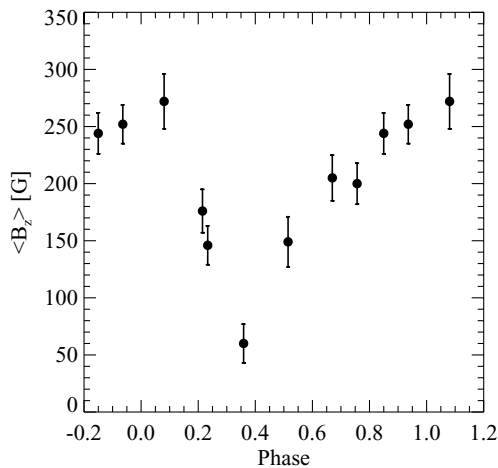
Figure 2. The mean longitudinal magnetic field $\langle B_z \rangle$ plotted over the rotational phase.

(Ritter & Washuettl 2004). This pipeline is based on IRAF and it does the standard reduction steps, i.e. bias-subtraction, flat-field correction, scattered light removal and optimal extraction of the spectral orders. Due to the overlapping orders, around 6000 Å and redder, the scattered light fit and the light pollution from adjacent orders are corrected using the HAMSCAT program (Churchill & Allen 1995).

A full list of observations together with the date, rotational phase, exposure time and S/N is given in Table 2.

3 SURFACE TEMPERATURE MAPPING

A surface temperature map of FK Com was obtained using the Doppler imaging technique. For the imaging, the Tikhonov Regularization code INVERS7PD, originally developed by N. Piskunov (see e.g. Piskunov et al. 1990) and modified by T. Hackman

Table 1. The mean longitudinal magnetic field measurements with FORS 1 over the rotational period. The quoted errors are 1σ uncertainties.

| Date	HJD	Phase	$\langle B_z \rangle$
08.04.12	54569.219 44	0.938	252 ± 17
08.04.13	54570.235 17	0.361	60 ± 17
08.04.15	54572.289 69	0.217	176 ± 19
08.04.19	54576.213 63	0.852	244 ± 18
08.04.20	54577.133 87	0.235	146 ± 17
08.04.21	54578.181 42	0.672	205 ± 20
08.04.22	54579.167 47	0.083	272 ± 24
08.04.23	54580.209 49	0.517	149 ± 22
08.04.26	54583.190 39	0.759	200 ± 18

Table 2. The high-resolution spectroscopy with SES at the STELLA observatory. The date of the observations, rotational phase and the S/N per resolution element are given.

Date	HJD	Phase	S/N
08.04.14	245 4571.378 91	0.046	116
08.04.15	245 4571.515 63	0.103	100
08.04.15	245 4571.636 72	0.153	116
08.04.15	245 4572.378 91	0.462	124
08.04.16	245 4572.667 97	0.583	101
08.04.16	245 4572.730 47	0.609	99
08.04.16	245 4573.378 91	0.879	126
08.04.16	245 4573.488 28	0.925	121
08.04.17	245 4573.656 25	0.995	134
08.04.17	245 4574.378 91	0.296	126
08.04.18	245 4574.585 94	0.382	109
08.04.18	245 4574.726 56	0.441	84
08.04.18	245 4575.406 25	0.724	132
08.04.19	245 4575.585 94	0.799	119
08.04.19	245 4575.699 22	0.846	123

(Hackman, Jetsu & Tuominen 2001), was used. The stellar parameters adopted for the Doppler imaging, and more details on the selection of the parameters, inversion technique and line-profile calculation, are given by Korhonen et al. (1999, 2007). In the inversions, the whole spectral region 6416–6444 Å was used, only the atmospheric line at 6433 Å was masked out. The temperature of the unspotted surface was set to 5200 K. This is somewhat higher than what is usually derived for FK Com, i.e. 5000 ± 50 K. The difference could be caused by problems with scattered light removal or by noisiness of the data.

The surface temperature map based on the STELLA data is shown in Fig. 3. The map shows two main active regions on the surface. One active region is spanning the phases 0.00–0.14 at an average latitude of 58°. This region has a minimum temperature of 3650 K, and it harbours the coolest spot seen on the surface for this time period. The other major spot concentration is located at phases 0.21–0.35. This active region has a minimum temperature of approximately 4300 K and it spans two latitude ranges, one at high latitudes with an average latitude of 61° and another one at the equator.

The case where two high-latitude spots of different contrasts are approximately 0.2 in phase apart is commonly seen on the surface of FK Com (see e.g. Korhonen et al. 2007). The large temperature difference of approximately 1500 K between the coolest spot and the unspotted surface in the present map is larger than the average difference seen on FK Com. Still, similar temperature differences have been reported before for some time periods, e.g. 2002 August (Korhonen et al. 2007). On the whole, the spot configuration seen
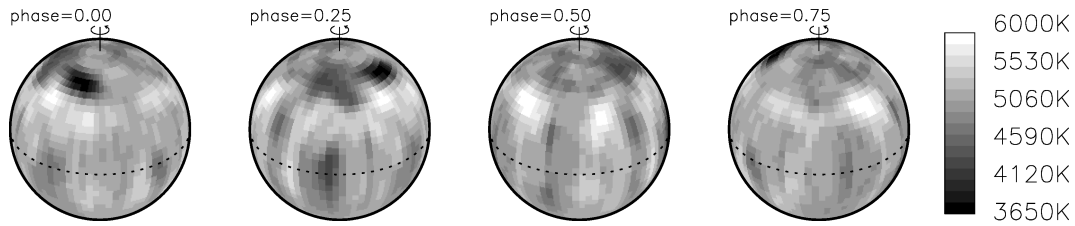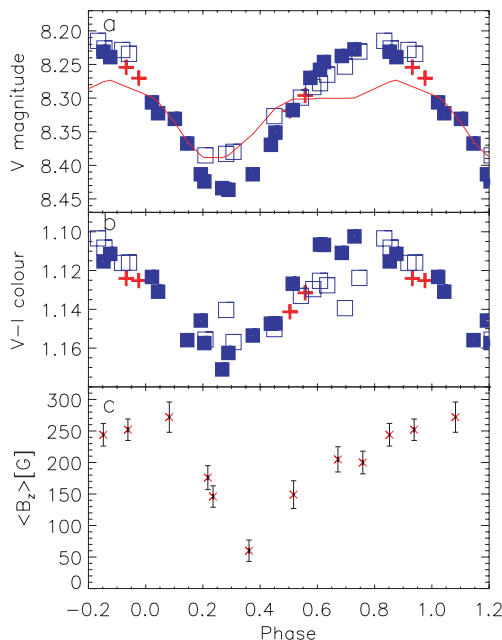
Figure 3. The surface temperature map of FK Com. The surface is shown at four different rotational phases which are 0.25 in phase apart. The grey-scale gives the temperature in kelvin.

in the current map is similar to what one would expect on FK Com based on the earlier Doppler imaging results.

4 DISCUSSION

4.1 Spot evolution in 2008 April–May

The *V*-band light curve is shown in Fig. 4a. It has a broad minimum spanning phases 0.1–0.4. In the *V*-band light curve, the crosses are from the same time period as the $\langle B_z \rangle$ measurements, filled squares from the 11 days preceding the magnetic field measurements and the open squares from the 13 days following the field measurements. Some spot evolution is seen in the light curve within the 38 days that the observations cover. The minimum gets broader and shallower with time. Unfortunately, we have only four measurements coinciding with the magnetic field measurements; thus, it is impossible to determine exactly the shape of the photometric minimum which
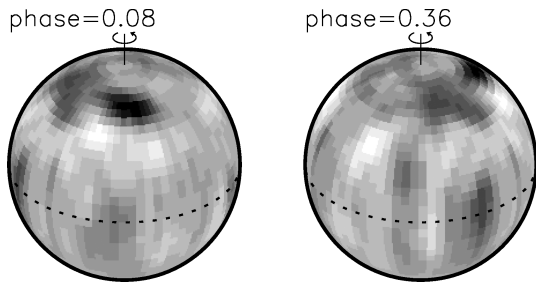
corresponds to our magnetic field determination. Still, even though the exact shape of the light-curve minimum has somewhat changed, the locations of the minimum and maximum have not changed for more than a month that the photometric observations cover. Thus, also our spectropolarimetric and spectroscopic observations that are overlapping in time, but spanning 14 and 4 days, respectively, can be studied together.

The solid line plotted in Fig. 4(a) is the *V*-band photometry calculated from the Doppler image, and shifted to the average magnitude of the *V*-band observations obtained before the magnetic field measurements. Clearly, the shape of the calculated light curve follows quite well the observed one. The main difference is detected in the amplitude of the light curve, i.e. the calculated curve has smaller amplitude. This indicates that the spots around 0.00–0.35, based on the photometry, should be larger or cooler than in the Doppler image. Another possible explanation for the small amplitude in the calculated light curve is that the areas around phases 0.5–0.8, which in the Doppler image are 400–500 K cooler than the unspotted surface and cause the dip seen in the calculated light curve at these phases, are actually artefacts. Overall, the comparison of the light curve calculated from the Doppler image and the observed *V*-band light curve indicates that the location of the main cool spots seen in the temperature map is correct.

The $V - I$ colour curve, also obtained by Amadeus, is shown in Fig. 4(b). It displays a similar shape as seen in the $\langle B_z \rangle$ variation curve and the *V*-band light curve. Unlike the *V* band, the $V - I$ colour does not show large differences in the shape of the minimum between the observations obtained before and after the magnetic field determination. This indicates that the relative temperature of the spotted regions remains the same. On the other hand, the $V - I$ colour obtained before and after the $\langle B_z \rangle$ measurements shows differences around the phases 0.6–0.8. From the *V*-band light curve, it can be seen that at these phases the star is consistently slightly fainter after our magnetic field observations than before them. This behaviour, together with the behaviour seen in the $V - I$ colour, indicates that there could be a new active region forming around phases 0.6–0.8.

4.2 Correlation between the magnetic field measurements and the star-spot location

As presented in Fig. 2, the mean longitudinal magnetic field $\langle B_z \rangle$ shows clear variations with the rotational phase. In Fig. 4, the magnetic field strength is plotted together with the *V*-band light curve and the $V - I$ colour curve. The photometric minimum, seen in the *V*-band light curve, $V - I$ colour and also determined from the Doppler image, occurs close to the minimum strength of the mean longitudinal magnetic field. The exact location of the $\langle B_z \rangle$ minimum appears slightly shifted with respect to the photometric minimum, and also the maximum of $\langle B_z \rangle$ occurs within the broad photometric

Figure 4. The *V*-band magnitudes, $V - I$ colour and mean longitudinal magnetic field strength plotted against the rotational phase. (a) *V*-band light curve. The crosses denote observations obtained during the same time period as the magnetic field measurement, filled squares show the observations obtained 11 d prior the magnetic field observations, and the open squares display observations from the following 13 days. The solid line gives the photometry calculated from the Doppler image, and shifted to the average magnitude of the *V*-band observations obtained before the $\langle B_z \rangle$ measurements. (b) $V - I$ colour. The symbols are the same as for the *V*-band light curve. (c) The mean longitudinal magnetic field.

Figure 5. As Fig. 3, but now showing the surface of FK Com at the phases of the maximum and minimum $\langle B_z \rangle$, phases 0.08 and 0.36, respectively.

minimum. Fig. 5 shows the surface temperature map centred at the two rotational phases that exhibit the $\langle B_z \rangle$ maximum and minimum. These plots clearly show that the coolest spot occurs at the phase of the field maximum, i.e. at phase 0.08, and that the field minimum of phase 0.36 coincides with the secondary active region seen on the surface.

It seems that the behaviour of $\langle B_z \rangle$ in FK Com is correlated with the star-spots seen on the surface, and that the main spot on the surface, at phase 0.1, has positive magnetic field polarity. The minimum of the magnetic field strength occurs around the active region of phase 0.3. The observed minimum could be explained by this active region having a negative magnetic field polarity. The negative field would partly cancel the positive field emerging in the dominant spot. This cancellation becomes more efficient when the dominant active region moves closer to the stellar limb, and the secondary active region approaches the centre of the disc. Therefore, the minimum of $\langle B_z \rangle$ is seen slightly shifted from the centre of the secondary active region, and also away from the dominant spot.

If the spot at the phase 0.1 has different polarity than the ones at 0.3, then this configuration closely resembles what is commonly observed in the sunspots. In the Sun, spots usually occur in pairs of different polarity, and the leading spot is compact and the following one fragmented. Thus, in Doppler images the leading spot would appear cooler, and the following one would have higher average temperature, as is also seen in the surface temperature map of FK Com. In the Sun, the spots are also connected by magnetic loops. Using the *Chandra* X-ray observations, Drake et al. (2008) find some indication for magnetic loops also on FK Com. Their observations suggest that the observed X-ray emission originates from plasma residing predominantly in extended structures centred at a phase halfway between two active regions, and that the coronal structures revealed by the *Chandra* observations correspond to magnetic fields joining these two active regions.

4.3 Chromospheric activity

For studying the possible connection between the chromospheric and photospheric activity on FK Com in 2008 April, the Hα line profiles obtained with STELLA I were also investigated. All the profiles from the 15 epochs observed in this study are plotted in Fig. 6. The radial velocity of FK Com, -24 km s^{-1} (Huenemoerder et al. 1993), has been removed from the profiles. In FK Com, the Hα line is a very strong and wide double-peaked emission line. The shape of the profile varies strongly with time, and especially the strength of the absorption core shows significant changes.

Earlier studies have explained the observed behaviour of Hα by structures similar to solar prominences. Based on the velocity behaviour of the Balmer lines studied by Huenemoerder et al. (1993),
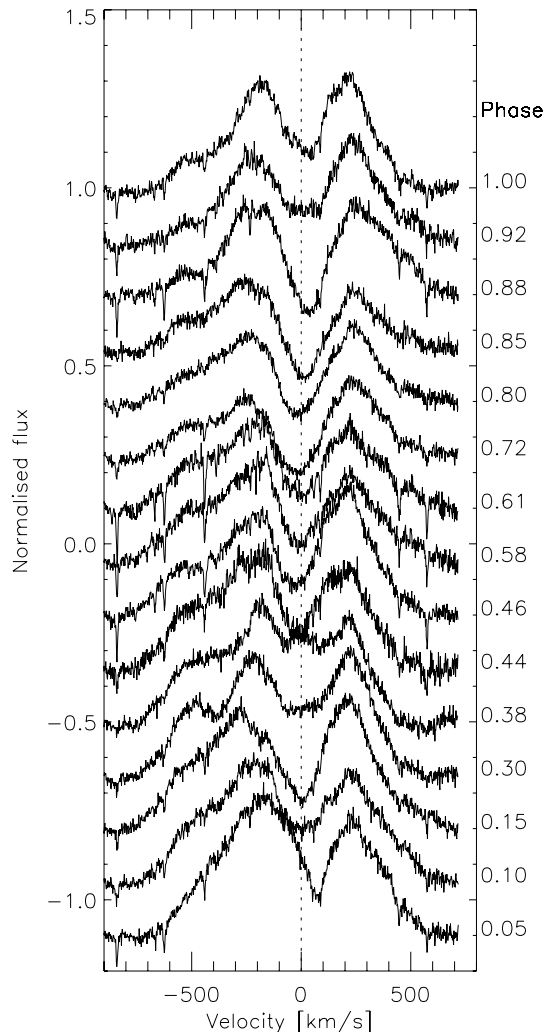

Figure 6. The Hα line variations in FK Com. All the 15 individual Hα observations obtained in this study are shown plotted against the velocity obtained in relation to the rest wavelength of the Hα.

the material in the prominences is confined within one stellar radius from the rotation axis. Welty et al. (1993) agree on the prominence theory and also conclude that their measurements can be explained by one single dominant emitting prominence. The work by Oliveira & Foing (1999) also supports the existence of prominences, but they find evidence for several different prominences existing simultaneously. On the other hand, Kjurkchieva & Marchev (2005) suggest that the origin of the Hα emission in FK Com is a disc, which is half-illuminated. They also suggest that the source of illumination is a low-mass hot secondary orbiting the disc.

For studying in detail the activity seen in the Hα line, a dynamic spectrum was constructed from the Hα profiles. This spectrum is shown in Fig. 7. Brighter the plot the more enhanced the emission is. The phases of the observations are shown with crosses on the plot. The data for the phases where there are no observations are interpolations between the closest phases with data. For showing the emission features better, another dynamic spectrum (Fig. 8) was created in which the profile showing the least chromospheric activity, phase 0.80, was subtracted from all the profiles.

The dynamic spectra clearly show that the phases close to the photospheric spots, i.e. 0.0–0.35, exhibit enhanced emission. At
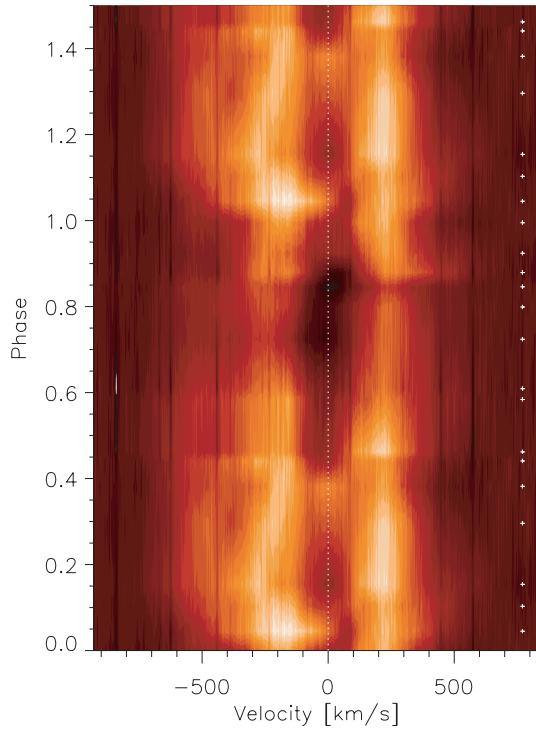
Figure 7. Dynamic spectrum of the Hα line of FK Com for 2008 April. The plot is shown from the phase 0.0 until 1.5 to better present the structure around the phase 1.0. The crosses on the right-hand side of the plot give the phases of the observations and the dashed line the zero velocity. Brighter the plot the more enhanced the emission is.
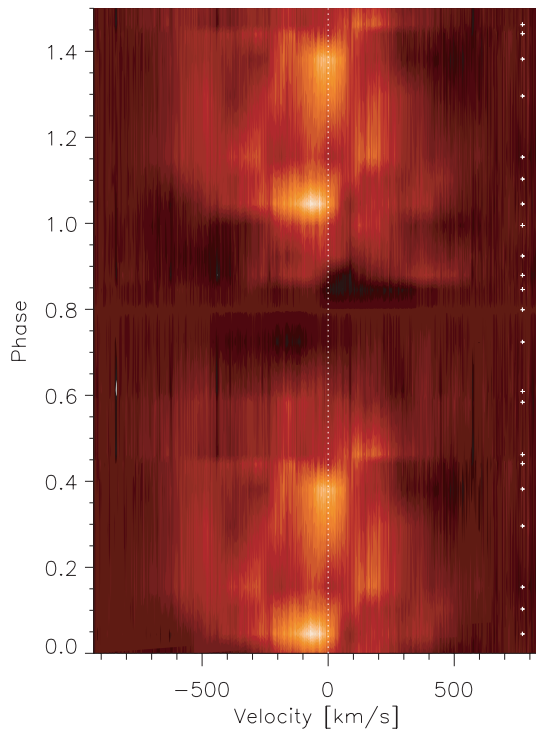
Figure 8. As in Fig. 7, but the profile showing the minimum chromospheric activity, phase 0.80, has been subtracted from all the profiles before creating the dynamic spectrum.
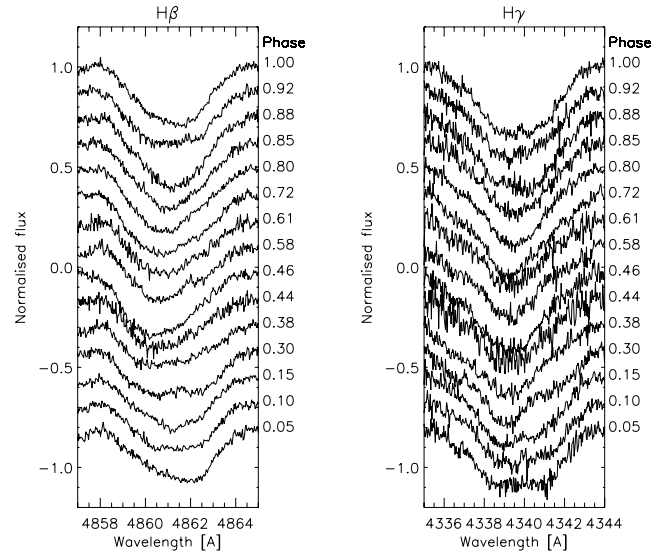

Figure 9. The Hβ and Hγ line variations in FK Com at all the 15 phases.

the phase 0.38, almost the whole absorption core gets filled with emission (clearly seen also in Fig. 6). This could be caused by a flare event originating close to the spot group around the phases 0.21–0.35, or by plage region rotating to the centre of the disc. As the He I D$_3$ line (5876 Å), which is often seen in emission in stellar flares (see e.g. Huenemoerder & Ramsey 1987; López-Santiago et al. 2003), does not show any emission during the observations, the flare is a less likely option. Additionally, the Hα profile at the phase 0.05 shows very strong emission, especially in the blue emission peak which extends to the red of the rest wavelength of Hα. Another intriguing structure in the line profiles is the increased emission at the velocity -550 km s^{-1}. This feature is very well seen at the phases 0.3–0.4, and is also present, to some extent, at most phases. It is also worth noting that the blue emission peak is wider than the red one, and often extends to velocities of -700 km s^{-1}, whereas the red peak usually only extends up to $+500$ km s^{-1}. The phases 0.60–0.85, during which the photospheric spots are hardly seen, show much less Hα emission than the other phases, and at these phases the central absorption core is also at its strongest.

To further investigate the chromosphere of FK Com, the behaviour of Hβ and Hγ lines was also investigated. As can be seen from Fig. 9, in FK Com Hβ and Hγ are absorption lines that show temporal variations. In the case of Hγ, the S/N is quite poor and the variations are not as easily seen as in Hβ. In both cases, the line is the deepest at phase 0.80, thus indicating the least amount of emission filling in the line core. When this line profile is subtracted from the other profiles, the excess emission at different phases can be studied. Fig. 10 shows the dynamical spectrum of the Hβ and Hγ excess emission. Both pictures are strikingly similar to the one seen in the case of Hα, especially in Hβ where the S/N is better. The phases where the photospheric spots are seen exhibit the most excess emission, and the chromosphere at the least spotted phases is again the least active.

The Hα, Hβ and Hγ observations clearly show that the chromosphere of FK Com is more active at the phases where the photospheric spots are located. In Hα, the strong double-peaked emission line is still present also at the phases in which the spots are not seen, but in these phases the emission peaks are less prominent and the absorption core is the deepest. On the whole, the Hα profile of the
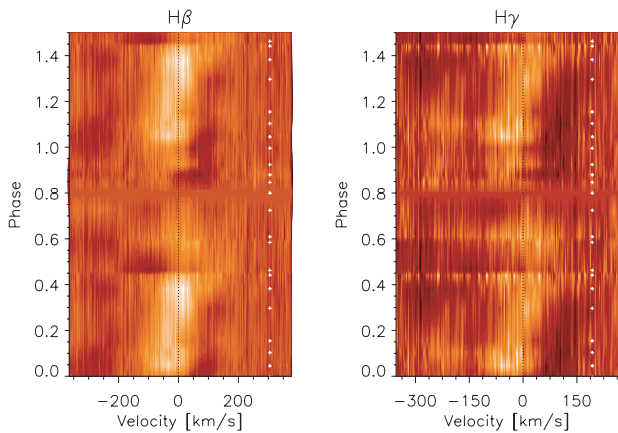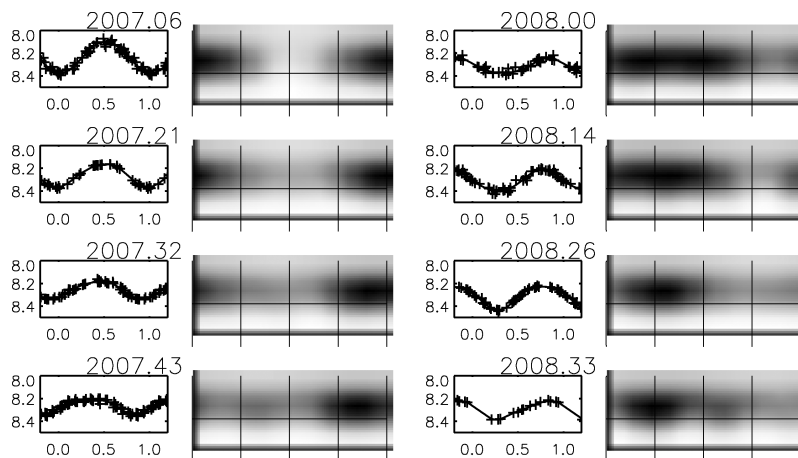
Figure 10. Dynamic spectrum of the excess emission in the Hβ and Hγ line. In both the cases, the profile showing the minimum chromospheric activity, phase 0.80, has been subtracted from all the profiles to create the excess emission profiles.

non-spotted phases has a shape that can be explained by a disc, and the spotted phases exhibit enhanced emission, seen also in the Hβ and Hγ profiles, which could originate from plages and prominences.

4.4 The magnetic field and the flip-flop phenomenon

In many active stars, the spots concentrate on two permanent active longitudes, which are 0.5 in phase apart (see e.g. Berdyugina & Tuominen 1998). In some of these stars, the dominant part of the spot activity concentrates on one of the active longitudes, and abruptly switches the longitude every few years. This so-called flip-flop phenomenon was first discovered in FK Com (Jetsu et al. 1993). Since the discovery, flip-flops have been reported in different types of stars, e.g. young solar-type stars (e.g. Järvinen et al. 2005), RS CVn binaries (e.g. Berdyugina & Tuominen 1998) and the Sun (Berdyugina & Usoskin 2003; Usoskin, Berdyugina & Poutanen 2005), even though this last result is still being debated (Pelt, Tuominen & Brooke 2005; Pelt et al. 2006).

The *V*-band photometry from 2007 to 2008 indicates that the latest flip-flop on FK Com has happened during the latter part of the year 2007. In Fig. 11, the *V*-band light curves are shown together with the

results from the light-curve inversions (see Korhonen, Berdyugina & Tuominen 2002). The results for 2007 show the main spot around phase 0.0 (or 1.0). In the last light-curve inversion from 2007, time period 2007.43, an indication of a spot forming approximately 0.5 in phase apart from the main spot is seen. The first light curve of 2008, 2008.00, which was obtained during 2007 December and 2008 January, shows a broad minimum around phase 0.0–0.5. During the beginning of 2008, the minimum became more concentrated and in the data from the time period 2008.26 one concentrated spot at the phase 0.25 is seen. This indicates that the active region observed between 2007 July and 2008 April has changed phase by 0.5 (from phase 0.75 to 0.25), and thus forming a flip-flop event.

The flip-flop phenomenon has strong implications for the dynamo theory. The behaviour of the global solar magnetic field can be explained by an axisymmetric mean-field dynamo without any longitudinal structure. In rapidly rotating stars, the higher-order non-axisymmetric modes become excited, forming two active regions that are 0.5 in phase apart (e.g. Moss et al. 1995), i.e. equivalent to the two permanent active longitudes. Not only is the magnetic configuration different in the axisymmetric and non-axisymmetric modes, but so are their oscillatory properties. The solar-type axisymmetric modes show clear cyclic behaviour, whereas the non-axisymmetric modes do not oscillate. To explain the flip-flop phenomenon, both properties, non-axisymmetric field configuration and oscillations, are needed. Recently, some attempts on modelling this behaviour have been published (e.g. Moss 2004; Elstner & Korhonen 2005). From a theoretical point of view, one of the key questions on the flip-flop phenomenon is: do spots on the two permanent active longitudes have different magnetic field polarities?

Our current spectropolarimetric observations suggest the existence of two cool spots seen on the surface having different polarities. Still, these two spots have to be considered to be located on the same active longitude as they together form the photometric minimum. Based on the photometric observations, the second active longitude should be around phase 0.75, and at that phase no negative magnetic field polarity is seen. Although, a very small dip in $\langle B_z \rangle$ is visible around the phase 0.75 which could be caused by a weak negative polarity field slightly cancelling the signal from the positive polarity.

One has to keep in mind that the observations presented in this work have low spectral resolution and do not provide a detailed

Figure 11. The light-curve inversion results obtained from the 2007–2008 *V*-band photometry. The left-hand panels show the observed light curve (crosses) and the inversion result (solid line). The right-hand panels are the spot filling factor maps, where a darker colour indicates larger filling factor. The equator and the phases 0.0, 0.25, 0.50, 0.75 and 1.0 are shown by solid lines in the filling factor maps.

insight into the magnetic surface structure as polarized line profiles of temperature and magnetic-field-sensitive lines cannot be studied individually. For properly answering the question on the spot polarities at the two permanent active longitudes, high-resolution spectropolarimetric observations would be needed. Also, these high-resolution observations should be carried out before and after a flip-flop event to study the possibility of the active longitudes changing polarity during the flip-flop, as suggested by Tuominen, Berdyugina & Korpi (2002).

5 CONCLUSIONS

The following conclusions can be drawn from the low-resolution spectropolarimetry, high-resolution spectroscopy and broad-band photometry presented in this work.

(i) The mean longitudinal magnetic field $\langle B_z \rangle$, measured in 2008 April, shows clear variations over the rotational phase of FK Com, with a maximum $\langle B_z \rangle = 272 \pm 24$ G at the phase 0.08 and the minimum $\langle B_z \rangle = 60 \pm 17$ G at the phase 0.36.

(ii) The contemporaneous determination of the star-spot locations by the Doppler imaging technique reveals three main spot groups on the surface of FK Com in 2008 April. Two groups are located at high latitudes close to $60°$, and one is located close to the equator. The separation of the high-latitude spot groups is 0.2 in phase.

(iii) Both the maximum and minimum value of $\langle B_z \rangle$ occur within the phases of the broad photometric minimum. The maximum value coincides with the cool high-latitude spot spanning the phases 0.00–0.14 and the minimum value with the high-latitude and equatorial spots around the phases 0.21–0.35. This behaviour could be explained by the active region around the phase 0.1 having positive magnetic field polarity and the less cool spots around phase 0.3 a magnetic field of negative polarity.

(iv) The Hα profiles show enhanced emission at the phases 0.0–0.4, coinciding with the photospheric spots. The phases 0.6–0.9, when the photospheric spots are hardly seen, show least emission and the strongest central absorption core. Similar behaviour is also seen in the Hβ and Hγ lines.

(v) We would like to emphasize that obtaining high-resolution spectropolarimetric observations of FK Com, preferably before and after a flip-flop event, would provide valuable observational constraints for flip-flop dynamos.

ACKNOWLEDGMENTS

REFERENCES

Appenzeller I. et al., 1998, The Messenger, 94, 1
Babcock H. W., 1960, ApJ, 132, 521
Berdyugina S. V., Tuominen I., 1998, A&A, 336, L25
Berdyugina S. V., Usoskin I. G., 2003, A&A, 405, 1121
Bopp B. W., Stencel R. E., 1981, ApJ, 247, L131
Chugainov P. F., 1966, IBVS, 172, 1
Churchill C. W., Allen S. L., 1995, PASP, 107, 193
Donati J.-F. et al., 2003, MNRAS, 345, 1145
Donati J.-F., Forveille T., Collier Cameron A., Barnes J. R., Delfosse X., Jardine M. M., Valenti J. A., 2006, Sci, 311, 633
Drake J. J., Chung S. M., Kashyap V., Korhonen H., Van Ballegooijen A., Elstner D., 2008, ApJ, 679, 1522
Elstner D., Korhonen H., 2005, AN, 326, 278
Granzer T., Reegen P., Strassmeier K. G., 2001, AN, 322, 325
Hackman T., Jetsu L., Tuominen I., 2001, A&A, 374, 171
Hubrig S., Kurtz D. W., Bagnulo S., Szeifert T., Schöller M., Mathys G., Dziembowski W. A., 2004, A&A, 415, 661
Hubrig S. et al., 2005, A&A, 440, L37
Hubrig S., Yudin R. V., Schöller M., Pogodin M. A., 2006a, A&A, 446, 1089
Hubrig S., North P., Schöller M., Mathys G., 2006b, AN, 327, 289
Huenemoerder D. P., Ramsey L. W., 1987, ApJ, 319, 392
Huenemoerder D. P., Ramsey L. W., Buzasi D. L., Nations H. L., 1993, ApJ, 404, 316
Järvinen S. P., Berdyugina S. V., Tuominen I., Cutispoto G., Bos M., 2005, A&A, 432, 657
Jetsu L., Pelt J., Tuominen I., 1993, A&A, 278, 449
Korhonen H., Berdyugina S. V., Hackman T., Duemmler R., Ilyin I. V., Tuominen I., 1999, A&A, 346, 101
Korhonen H., Berdyugina S. V., Tuominen I., 2002, A&A, 390, 179
Korhonen H., Berdyugina S. V., Hackman T., Strassmeier K. G., Tuominen I., 2007, A&A, 476, 881
Kjurkchieva D. P., Marchev D. V., 2005, A&A, 434, 221
Landstreet J. D., 1992, A&AR, 4, 35
López-Santiago J., Montes D., Fernández-Figueroa M. J., Ramsey L. W., 2003, A&A, 411, 489
Marsden S. C., Donati J.-F., Semel M., Petit P., Carter B. D., 2006, MNRAS, 370, 468
Merrill P. W., 1948, PASP, 60, 382
Moss D., 2004, MNRAS, 352, L17
Moss D., Barker D. M., Brandenburg A., Tuominen I., 1995, A&A, 294, 155
Oliveira J. M., Foing B. H., 1999, A&A, 343, 213
Pelt J., Tuominen I., Brooke J. M., 2005, A&A, 429, 1093
Pelt J., Brooke J. M., Korpi M. J., Tuominen I., 2006, A&A, 460, 875
Petit P. et al., 2004, MNRAS, 351, 826
Piskunov N. E., Tuominen I., Vilhu O., 1990, A&A, 230, 363
Ritter A., Washuettl A., 2004, AN, 325, 663
Semel M., 1989, A&A, 225, 456
Strassmeier K. G., Bartus J., Cutispoto G., Rodonò M., 1997, A&AS, 125, 11
Strassmeier K. G. et al., 2004, AN, 325, 527
Tuominen I., Berdyugina S. V., Korpi M. J., 2002, AN, 323, 367
Usoskin I. G., Berdyugina S. V., Poutanen J., 2005, A&A, 441, 347
Vogt S. S., Penrod G. D., Hatzes A. P., 1987, ApJ, 321, 496
Weber M., Granzer Th., Strassmeier K. G., Woche M., 2008, Proc. SPIE, 7019, 70190
Welty A. D., Ramsey L. W., Iyengar M., Nations H. L., Buzasi D. L., 1993, PASP, 105, 1427

This paper has been typeset from a TeX/LaTeX file prepared by the author.